



THE UNIVERSITY *of* EDINBURGH

Edinburgh Research Explorer

Mechanisms and Materials for NTE

Citation for published version:

Attfield, JP 2018, 'Mechanisms and Materials for NTE', *Frontiers in chemistry*, vol. 6.
<https://doi.org/10.3389/fchem.2018.00371>

Digital Object Identifier (DOI):

[10.3389/fchem.2018.00371](https://doi.org/10.3389/fchem.2018.00371)

Link:

[Link to publication record in Edinburgh Research Explorer](#)

Document Version:

Peer reviewed version

Published In:

Frontiers in chemistry

General rights

Copyright for the publications made accessible via the Edinburgh Research Explorer is retained by the author(s) and / or other copyright owners and it is a condition of accessing these publications that users recognise and abide by the legal requirements associated with these rights.

Take down policy

The University of Edinburgh has made every reasonable effort to ensure that Edinburgh Research Explorer content complies with UK legislation. If you believe that the public display of this file breaches copyright please contact openaccess@ed.ac.uk providing details, and we will remove access to the work immediately and investigate your claim.



Mechanisms and Materials for NTE

J. Paul Attfield^{1*}

¹ Centre for Science at Extreme Conditions and School of Chemistry, University of Edinburgh., Mayfield Road, Edinburgh EH9 3JZ, UK.

* Correspondence:

Prof. J. P. Attfield
j.p.attfield@ed.ac.uk

Keywords: thermal expansion, negative thermal expansion, thermal expansion coefficient, structural NTE, electronic NTE, morphological NTE

Abstract

Negative thermal expansion (NTE) upon heating is an unusual property but is observed in many materials over varying ranges of temperature. A brief review of mechanisms for NTE and prominent materials will be presented here. Broadly there are two basic mechanisms for intrinsic NTE within a homogenous solid; structural and electronic. Structural NTE is driven by transverse vibrational motion in insulating framework-type materials e.g. ZrW_2O_8 and ScF_3 . Electronic NTE results from thermal changes in electronic structure or magnetism and is often associated with phase transitions. A classic example is the Invar alloy, $\text{Fe}_{0.64}\text{Ni}_{0.36}$, but many exotic mechanisms have been discovered more recently such as colossal NTE driven by Bi–Ni charge transfer in the perovskite BiNiO_3 . In addition there are several types of NTE that result from specific sample morphologies. Several simple materials, e.g. Au, CuO, are reported to show NTE as nanoparticles but not in the bulk. Microstructural enhancements of NTE can be achieved in ceramics of materials with anisotropic thermal expansion such as beta-eucryptite and Ca_2RuO_4 , and artificial NTE metamaterials can be fabricated from engineered structures of normal (positive) thermal expansion substances.

1 Introduction

NTE (negative thermal expansion) refers to the unusual phenomenon of volume contraction upon heating. Although most materials display positive thermal expansion (PTE) on heating, NTE is found in a wide variety of substances over varying ranges of temperature. This brief review is an attempt to summarise the mechanisms and prominent materials that show NTE. Further details may be found in more substantial reviews published by other authors in recent years [1–6] and in the other papers in this special issue.

Control of thermal expansion is important for many applications from ceramic cooker hobs to housings for optical devices, with zero thermal expansion (ZTE) materials or composites of PTE and NTE components being particularly useful. Thermal expansion is quantified through the linear or volume (bulk) thermal expansion coefficients (TECs), $\alpha_L = (1/L)(dL/dT)$ and $\alpha_V = (1/V)(dV/dT)$, which respectively measure the change in length L or volume V of an object with temperature T . α_L and α_V are typically quoted in 10^{-6} K^{-1} units, equivalent to ppm (parts per million) K^{-1} or MK^{-1} . Isotropic substances such as simple liquids, glasses, polycrystalline ceramics, and cubic crystals, have the same α_L in all directions with $\alpha_V = 3\alpha_L$. ZrW_2O_8 is a famous example of a cubic NTE material [7]. However uniaxial (tetragonal, hexagonal or trigonal) crystals may have different linear

TECs α_{\parallel} and α_{\perp} parallel and perpendicular to the unique symmetry axis, respectively, and crystals with orthorhombic or lower symmetry have three different values α_1 , α_2 and α_3 in mutually perpendicular directions. The volume TEC is given by $\alpha_V = \alpha_{\parallel} + 2\alpha_{\perp}$ or $\alpha_V = \alpha_1 + \alpha_2 + \alpha_3$ and when the linear TECs are very different, such as a mix of negative and positive values, then highly anisotropic thermal expansion may be obtained. TECs of crystalline materials are usually measured by determining how unit cell lengths change with temperature from diffraction measurements. Direct strain gauge (dilatometry) measurements of crystals can also be used, and are particularly useful for ceramics and amorphous materials such as glasses. Diffraction and dilatometry expansion measurements can give different results due to the effects of microstructure, as discussed in Section 3.2.

NTE materials have negative α_V over some temperature range. Reported α_V values vary from -1 to $-1000 \times 10^{-6} \text{ K}^{-1}$, but it is also important to consider the temperature range to which the quoted α_V refers as very large negative α_V 's may result from modest volume decreases over very narrow temperature ranges at a phase transition. For this reason it is often more useful to consider the overall volume decrease; materials with $-\Delta L/L > 1\%$ and so $-\Delta V/V > 3\%$ have notably large NTE.

The thermodynamic origin of thermal expansion in solids is expressed through the relation $\alpha_V = \gamma C_V/BV$ where C_V is heat capacity at constant V , $B = -V(dp/dV)$ is the bulk modulus with p being pressure, and γ is the weighted or macroscopic Grüneisen parameter summed over values for the active phonon frequencies ω_i as $\gamma_i = -d(\ln \omega_i)/d(\ln V)$. C_V and B always take positive values, hence variations in the sign of α_V arise from corresponding variations in the sign of γ . NTE is often associated with other unusual lattice properties such as negative linear compressibility under applied pressure [6] and pressure-induced softening where dB/dp becomes negative [2].

Conventional PTE arises because γ is usually positive as a consequence of the shape of the interatomic potential for bonding between two atoms, as shown in Fig. 1. Anharmonicity in the shape of the potential leads to an increase in the average interatomic distance as higher vibrational states become more populated as temperature rises. As this pairwise potential shape applies qualitatively to all type of chemical bonding, it might appear that PTE should be a universal behaviour, but NTE can arise from two ‘escapes’ that circumvent the latter argument.

2 Intrinsic NTE mechanisms

2.1 Structural NTE

The first ‘escape’ from the universal PTE behaviour expected from the interatomic potential in Fig. 1 arises from the more complex vibrational properties of large arrays of atoms. Fig. 2 shows some of the possible motions for a chain of atoms. Longitudinal (L) vibrations in the direction of the bonds (Fig. 2(a)) tend to lengthen the chain as temperature increases through thermal expansion of the individual bonds via the anharmonicity of the interatomic potential (Fig. 1). However, transverse (T) motions perpendicular to the direction of the chain tend to shorten the chain-length as the amplitude of vibration increases with temperature (Figs. 2(b) and (c)) and so can lead to NTE. This is sometimes known as the tension or ‘guitar string’ effect. Lattice vibrations, also known as phonons, are usefully classified as optic (O) with short wavelengths and high frequencies and energies, or acoustic (A) with long wavelengths and low frequencies and energies. Transverse optic (TO) phonons like that shown in Fig. 2(b) lead to large chain shortening (NTE) but may only be excited at high temperatures in view of their high energies, whereas transverse acoustic (TA) modes that lead to more modest NTE are excited at lower temperatures. Detailed theoretical and experimental analyses

of phonon spectra are needed to assess the contributions of TO and TA vibrations to the NTE of real materials [2,6].

Structural NTE results when the shortening effects of the transverse phonon amplitudes due to bending or torsional motions outweigh the expansion effects of the longitudinal modes. Low atomic connectivity so that atoms have free space to move into during transverse motions leading to large amplitudes is a necessary feature for NTE to prevail. Planar 3-coordination is the maximum connectivity known to lead to negative expansion, as exemplified by graphene sheets of carbon atoms [8]. However when these sheets are stacked in the three-dimensional lattice of graphite, conventional PTE arising from soft van der Waals bonding potentials in the stacking (high symmetry) direction gives a large $\alpha_{\parallel} = 23.1 \times 10^{-6} \text{ K}^{-1}$ that outweighs the NTE in the perpendicular directions ($\alpha_{\perp} = -0.6 \times 10^{-6} \text{ K}^{-1}$) leading to bulk PTE ($\alpha_V = \alpha_{\parallel} + 2\alpha_{\perp} = 21.9 \times 10^{-6} \text{ K}^{-1}$) [9].

Bulk structural NTE requires a large proportion of 2-coordinate linker groups, connecting more highly-coordinated atoms into a three-dimensional structure. Some representative examples of structural NTE material types, with 2-connected linkers underlined, are ScF_3 , Ag_2O , ZrW_2O_8 , ZrV_2O_7 , LiAlSiO_4 (the mineral β -eucryptite), zeolitic forms of SiO_2 (e.g. ITQ-4) and related AlPO_4 (e.g. AlPO_4 -17) frameworks, $\text{Cd}(\text{CN})_2$, $\text{Co}_3[\text{Co}(\text{CN})_6]_2$, and metal organic frameworks such as IRMOF-1 ($\text{Zn}_4\text{O}(\text{bdc})_3$, where bdc is 1,4-benzodicarboxylate). These have α_V values of magnitude -20 to $-120 \times 10^{-6} \text{ K}^{-1}$ over typical temperature ranges of a few hundred K; details and citations are shown in [2]. All of these materials have the majority of their atoms in the 2-connected linkers. The metal fluoride and oxide examples have 2-coordinate atoms linking tetrahedral or octahedral units together. These polyhedra tend to be rigid so the transverse vibrations of the lattice may be described in the rigid unit mode (RUM) picture [2].

The importance of the transverse motions of the linker atoms or groups to NTE is further demonstrated by changes observed when additional molecules or ions are inserted into NTE materials. The inserted species within cavities in the structure are adjacent to the linkers and so reduce the amplitudes of their transverse vibrations. Redox insertion of only 6% Li into Fe-doped ScF_3 switches the TEC from negative to positive [10], and the same change is found when K^+ or H_2O is inserted into the channels of the cyanide framework material $\text{YFe}(\text{CN})_6$ [11].

2.2 Electronic NTE

A disparate group of materials, usually dense metal alloys or ceramics, display NTE that is not driven by the structural (transverse vibration) mechanism. Although they have a wide variety of physical properties, and so are sometimes described as having different NTE mechanisms, they have the common feature that NTE results from thermal changes in the interatomic bonding potential, as illustrated in Fig. 3. Changes in bonding with temperature such that the interatomic potential becomes more strongly bonding can shift the curve to a smaller equilibrium distance at higher temperature. This may occur through a relatively sharp first order phase transition between two distinct states, or the potential may gradually evolve with changing temperature through a second or higher order transition. When the effect of this ‘escape’ outweighs the usual PTE from the anharmonicity of the potentials then NTE may be observed over temperature range of the crossover.

Fig. 4 illustrates the schematic changes in lattice volume with temperature for a material displaying electronic NTE. Both the larger-volume low- T and the smaller-volume high- T states shown in Fig. 3 display conventional PTE behaviour, but the change between them in the crossover region with lower and upper temperatures T_l and T_u leads to NTE. T_u often marks an ordering temperature such as a magnetic or ferroelectric Curie transition, and the lower limit T_l is reached where the order parameter (magnetisation or electric polarisation) is fully saturated. In other cases such as charge transfer

materials, T_l and T_u mark the lower and upper limits of the two-phase region where the low- T and high- T phases coexist. The electronically-induced excess volume ΔV_{ex} relative to the extrapolated volume of the high- T state, V_{HT} , may be used to calculate the spontaneous volume striction $\Delta V_{\text{ex}}/V_{\text{HT}}$. Variations in the magnitude of ΔV_{ex} and the separation between T_l and T_u may be used to tune electronic materials from reduced PTE, through ZTE to NTE behaviour. A famous material that launched the study of unusual thermal expansion properties is the Invar alloy $\text{Fe}_{0.64}\text{Ni}_{0.36}$ named for an *invariant* length with a very small $\alpha_L = 1 \times 10^{-6} \text{ K}^{-1}$ (effectively ZTE) below magnetic $T_C = 500 \text{ K}$.

The transitions or changes that give rise to electronic NTE are usually associated with an increase in electron delocalisation on passing from the low- T to the high- T phase. The low- T phase is more electron localised or correlated (e.g. magnetically ordered), due to electron-electron repulsions that may be described by the Hubbard U energy, while the more electron delocalised or disordered high- T phase is stabilised by entropy. Electrons near the Fermi level are often in d- or f-states that are non-bonding or weakly antibonding, so their delocalisation allows the bonding potential to become more negative and shift to shorter distance as shown in Fig. 3.

Classes of materials where electronic NTE is found are;

- Metallic magnets, notably the Invar alloy above, also R_2Fe_{17} (R = rare earth) and related intermetallics, the permanent magnet family $\text{R}_2\text{Fe}_{14}\text{B}$, the $\text{Mn}_3(\text{Cu}, \text{Ge})\text{N}$ antiperovskites, and metallic perovskite oxides SrRuO_3 and manganites such as $\text{La}_{0.8}\text{Ba}_{0.2}\text{MnO}_3$. NTE is usually observed over a wide temperature range below the magnetic Curie transition.
- Insulating magnets – these generally do not show NTE but some examples are found for frustrated spinels e.g. CdCr_2O_4 and CdCr_2S_4 , the multiferroic $\text{Pb}(\text{Fe}_{0.5}\text{Nb}_{0.5})\text{O}_3$, and orbitally ordered MnF_3 below their Curie or Néel temperatures.
- Charge transfer materials, e.g. $\text{Bi}_{0.95}\text{La}_{0.05}\text{NiO}_3$, $\text{LaCu}_3\text{Fe}_4\text{O}_{12}$, $\text{Sm}_{0.67}\text{Y}_{0.33}\text{S}$, $\text{Sm}_{2.75}\text{C}_{60}$, and $\text{Yb}_8\text{Ge}_3\text{Sb}_5$, can show very large NTE resulting from volume collapses at metal to insulator charge transfer transitions. $\text{Bi}_{0.95}\text{La}_{0.05}\text{NiO}_3$ has $\alpha_V = -410 \times 10^{-6} \text{ K}^{-1}$ between 300 and 370 K, termed colossal NTE (CNTE). The oxides have intermetallic Bi/Ni or Cu/Fe charge transfer transitions, whereas electrons released through the ionisation process $\text{R}^{2+} \rightarrow \text{R}^{3+} + \text{e}^-$ in the $\text{R} = \text{Sm}, \text{Yb}$ materials are delocalised in the conduction band at high temperatures. NTE in V_2OPO_4 where charge ordering occurs without a metal-insulator transition was recently reported [12].
- Orbital ordering transitions usually associated with first-order Jahn-Teller distortions give rise to NTE in several materials. Ca_2RuO_4 has orbital order associated with a metal-insulator transition, while insulating LaMnO_3 which is much studied as the parent phase of the perovskite manganites undergoes a 0.4 % cell volume decrease at 750 K where the orbital order-disorder transition occurs.
- Ferroelectrics associated with off-centre displacements of cations to give a net polarisation sometimes show NTE below their Curie transitions. Prominent examples are perovskite oxides of lead with transition metal cations showing a second-order Jahn-Teller effect such as PbTiO_3 , $\text{Pb}(\text{Mg}_{0.33}\text{Ta}_{0.67})\text{O}_3$, and $\text{Pb}(\text{Fe}_{0.5}\text{Nb}_{0.5})\text{O}_3$. Cooling below T_C leads to a change from symmetric $\text{O}-\text{M}-\text{O}-\text{M}-\text{O}$ to asymmetric $\text{O} \cdots \text{M}-\text{O} \cdots \text{M}-\text{O}$ chains of atoms leading to polarity in the chain direction. The lengthening of $\text{O} \cdots \text{M}$ bonds where electrons are localised in antibonding states outweighs the shortening of the $\text{M}-\text{O}$ bonds, leading to a net expansion in the polar chain direction on cooling and hence the excess volume associated with NTE below T_C . This can lead to very large volume collapses on warming, for example, $\text{Pb}_{0.8}\text{Bi}_{0.2}\text{VO}_3$ shows $\Delta V/V = -7.9\%$ around $T_C \approx 600 \text{ K}$ [13].
- Superconductors sometimes show an excess volume and NTE below their critical temperatures T_c , for example in MgB_2 , $\text{La}_{1.85}\text{Sr}_{0.15}\text{CuO}_4$, and $\text{NdFeAsO}_{0.89}\text{F}_{0.11}$. Electron-

phonon coupling is directly implicated in the superconducting mechanism for BCS-type MgB_2 , whereas the latter two materials are unconventional superconductors where a magnetic pairing mechanism may be important. Loss of bonding electron density at the Fermi level due to electron-pairing below T_c is the general cause of NTE in superconductors.

Further details and citations when not shown above are given in the comprehensive review of NTE in functional materials by Chen et al [1].

3 Morphological NTE

The structural and electronic mechanisms for NTE described above apply to chemically homogenous materials such as a single crystal. However, there are further instances where NTE can arise or differ from the normal bulk behaviour due to the specific morphology of the sample.

3.1 Nanoparticle NTE

A variety of materials that show bulk PTE have been found to display NTE when prepared as small particles, usually in the nanoscale regime. For example, the magnetic insulators CuO and MnF_2 show PTE in the bulk but as 5 nm particles they display NTE below their Néel temperatures. CuO has a giant NTE of $\alpha_V = -110 \times 10^{-6} \text{ K}^{-1}$ between 20 and 170 K [14]. Nanoparticles of Au [15] and TiO_2 [16] are also reported to display NTE.

The origin of nanoparticle NTE is usually electronic as, for example, the excess volume of CuO particles above follows the general behaviour shown in Fig. 4. Localisation of ordered or correlated states tends to be enhanced at and near surfaces so the associated lattice expansion on cooling can dominate the overall behaviour in small particles with a large proportion of surface atoms. The structural NTE mechanism could also play a part as surface atoms have a lower connectivity than the bulk so transverse vibrational amplitudes may be enhanced.

3.2 Microstructural NTE

Direct measurement of α_V for ceramic samples sometimes gives a more negative value than that expected from crystallographic measurement of the linear TECs. The excess negative expansion is achieved by reducing the volumes of microcracks or voids within the ceramic on heating, as illustrated schematically in Fig. 5. Microstructural NTE was reported in an early study of β -eucryptite (LiAlSiO_4) [17] and very large effects have recently been discovered in Ca_2RuO_4 [18]. These ceramic materials both have anisotropic thermal expansion with one strongly negative coefficient that dominates the expansion of their ceramics. For example, on heating from 150 to 340 K, the orthorhombic a , b , and c axes of Ca_2RuO_4 show length changes of -0.6 , -5.0 , and $+4.5\%$ respectively, so an overall $\Delta V/V = -1.1\%$ is expected. However an 80% dense ceramic sample gave $\Delta V/V = -6.7\%$ revealing a substantial microstructural NTE effect.

Anisotropic thermal expansion leads to stresses at grain boundaries that result in microcracking in β -eucryptite ceramics on cooling to room temperature after sintering. Reduction of the microcrack volumes on subsequent heating results in bulk NTE and an enhancement of the excess NTE with increasing grain size (and hence internal microcrack volume) has been established [19]. However, this is less problematic for Ca_2RuO_4 -based ceramics, which have been combined with epoxy resin to generate ZTE materials that are stable to microcracking on thermal cycling [20].

3.3 Metamaterials NTE

Artificial structures consisting of two or more materials with different TECs (which may all be positive) can be engineered to contract when heating. A simple example based on bonded strips of two materials with different positive TECs is shown in Fig. 6. The structure contracts on heating through reduction of the volume of internal voids, which outweighs the increase in volume of the materials themselves. Designs for three-dimensional cellular metamaterials with varying TECs based on the use of such bimaterial connectors were proposed by Lakes [21].

Recent developments in additive manufacturing through three-dimensional printing technologies have enabled metamaterials with bulk NTE to be generated. In a recent example, a two-component polymer metamaterial showed bulk negative expansion with $\alpha_L = -50 \times 10^{-6} \text{ K}^{-1}$ although the individual components had PTE with an average $\alpha_L = 40 \times 10^{-6} \text{ K}^{-1}$ [22].

4 Summary

Although many diverse examples of NTE materials are reported, they may be classified according to two types of intrinsic mechanism. Electronic NTE arises from reduction in first-neighbour distances upon heating due to changes in the interatomic potential. These changes may arise from a variety of physical property transitions such as magnetism, charge transfer, ferroelectricity and superconductivity that alter the distribution of electron density. Structural NTE occurs through reduction in second- or higher- neighbour distances upon heating due to dominant effects of transverse vibrations such as bending or torsional modes, and is found in many framework-type materials with a high proportion of 2-connected linkers.

The intrinsic NTE mechanisms may be enhanced in nanoparticles, most likely through electronic effects from localisation of ordered or correlated states near surfaces. Further morphological mechanisms for NTE of bulk artefacts result from reducing the volume of internal voids upon heating. Microstructural NTE is found for ceramics of materials having anisotropic thermal expansion coefficients. Artificial structures of substances with different expansion coefficients may be used to generate metamaterials with NTE even when the individual components have PTE behaviour.

5 Conflict of Interest

The author declares that the research was conducted in the absence of any commercial or financial relationships that could be construed as a potential conflict of interest.

6 Author Contributions

This paper was written solely by the author.

7 Funding

The author acknowledges financial support from EPSRC.

8 Acknowledgments

This paper is based upon a talk presented at the 2nd International Symposium on Negative Thermal Expansion and Related Materials (ISNTE-II) at Tokyo Institute of Technology, Yokohama, Japan in December 2017. The author thanks the organisers and participants for their contributions that helped to shape the ideas presented in this paper.

9 References

1. Chen, J., Hu, L., Deng, J., and Xing, X. (2015). Negative thermal expansion in functional materials: controllable thermal expansion by chemical modifications. *Chem. Soc. Rev.* 44, 3522-3567.
2. Dove, M. T., and Fang, H. (2016). Negative thermal expansion and associated anomalous physical properties: review of the lattice dynamics theoretical foundation. *Rep. Prog. Phys.* 79, 066503.
3. Lind, C. (2012). Two decades of negative thermal expansion research: where do we stand? *Materials* 5, 1125-1154.
4. Takenaka, K. (2012). Negative thermal expansion materials: technological key for control of thermal expansion. *Sci. Technol. Adv. Mater.* 13, 013001.
5. Liu, Z. N., Gao, Q. L., Chen, J., Deng, J. X., Lin, K., and Xing, X. R. (2018). Negative thermal expansion in molecular materials. *Chem. Commun.* 54, 5164-5176.
6. R. Mittal, R., Gupta, M. K, and Chaplot, S. L. (2018). Phonons and anomalous thermal expansion behavior in crystalline solids. *Prog. Materials Sci.* 92, 360-445.
7. Mary, T.A., Evans, J.S.O., Vogt, T., and Sleight, A.W. (1996) Negative thermal expansion from 0.3 to 1050 Kelvin in ZrW_2O_8 . *Science* 272, 90-92.
8. Yoon, D., Son, Y.-W., and Cheong, H. (2011). Negative thermal expansion coefficient of graphene measured by Raman spectroscopy. *Nano Lett.* 11, 3227-3231.
9. Morgan, W. C. (1972) Thermal expansion coefficients of graphite crystals. *Carbon* 10, 73-79.
10. Chen, J., Gao, Q., Sanson, A., Jiang, X., Huang, Q., Carnera, A., et al. (2017). Tunable thermal expansion in framework materials through redox intercalation. *Nature Commun.* 8, 14441.
11. Gao, Q., Chen, J., Sun, Q., Chang, D., Huang, Q., Wu, H., et al. (2017). Switching Between Giant Positive and Negative Thermal Expansions of a $\text{YFe}(\text{CN})_6$ -based Prussian Blue Analogue Induced by Guest Species. *Angew. Chem. Int. Ed.* 56, 9023-9028.
12. Pachoud, E., Cumby, J., Lithgow, C. T., and Attfield, J. P. (2018). Charge order and negative thermal expansion in V_2OPO_4 . *J. Am. Chem. Soc.* 140, 636-641.
13. Yamamoto, H., Imai, T., Sakai, Y., and Azuma, M. (2018). Colossal negative thermal expansion in electron-doped PbVO_3 perovskites. *Angew. Chem. Int. Ed.* 57, 1-5.
14. Zheng, X. G., Kubozono, H., Yamada, H., Kato, K., Ishiwata, Y., and Xu, C. N. (2008). Giant negative thermal expansion in magnetic nanocrystals. *Nature Nanotechnol.* 3, 724-726.
15. Li, W. H., Wu, S. Y., Yang, C. C., Lai, S. K., Lee, K. C., Huang H. L., et al. (2002). Thermal Contraction of Au Nanoparticles. *Phys. Rev. Lett.* 89, 135504.
16. Zhu, H., Li, Q., Ren, Y., Fan, L., Chen, J., Deng, J., et al. (2016). Hydration and thermal expansion in anatase nanoparticles. *Adv Mater.* 28, 6894-6899.
17. Gillery, F. H., and Bush, E. A. (1959). Thermal contraction of β -Eucryptite-. ($\text{Li}_2\text{O} \cdot \text{Al}_2\text{O}_3 \cdot 2\text{SiO}_2$) by X-Ray and dilatometer methods. *J. Am. Cer. Soc.* 42, 175-177.
18. Takenaka, K., Okamoto, Y., Shinoda, T., Katayama, N., and Sakai, Y. (2017). Colossal negative thermal expansion in reduced layered ruthenate. *Nature Comm.* 8, 14102.

19. Pelletant, A., Reveron, H., Ch  valier, J., Fantozzi, G., Blanchard, L., Guinot, F., and Falzon, F. (2012). Grain size dependence of pure β -eucryptite thermal expansion coefficient. *Mater. Lett.* 66, 68-71.
20. Takenaka, K., Shinoda, T., Inoue, N., Okamoto, Y., Katayama, N., Sakai, Y., et al (2017). Giant negative thermal expansion in Fe-doped layered ruthenate ceramics. *Appl. Phys. Express* 10, 115501.
21. Lakes, R. (2007). Cellular solids with tunable positive or negative thermal expansion of unbounded magnitude. *Appl. Phys. Lett.* 90, 221905.
22. Qu, J., Kadic, M., Naber, A., and Wegener, M. (2017). Micro-structured two-component 3D metamaterials with negative thermal-expansion coefficient from positive constituents. *Sci. Rep.* 7, 40643.

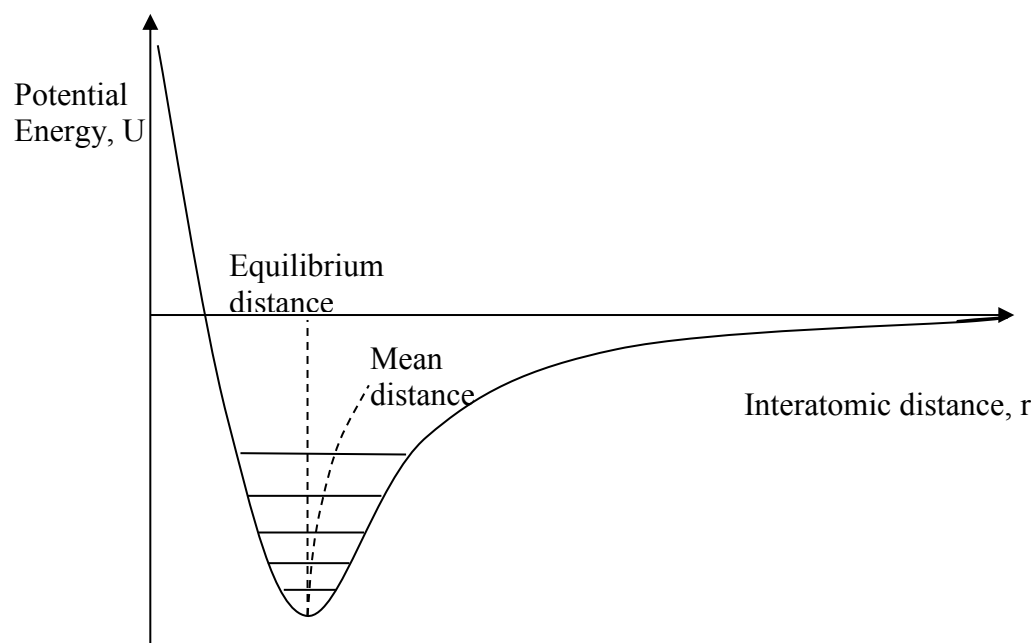


Fig. 1 The interatomic bonding potential, showing the variation of potential energy with interatomic distance for a pair of bonded atoms. Vibrational energy levels are quantised and with increasing temperature the occupation of higher levels leads to a slight increase in the mean interatomic distance relative to the minimum-energy equilibrium distance as shown.

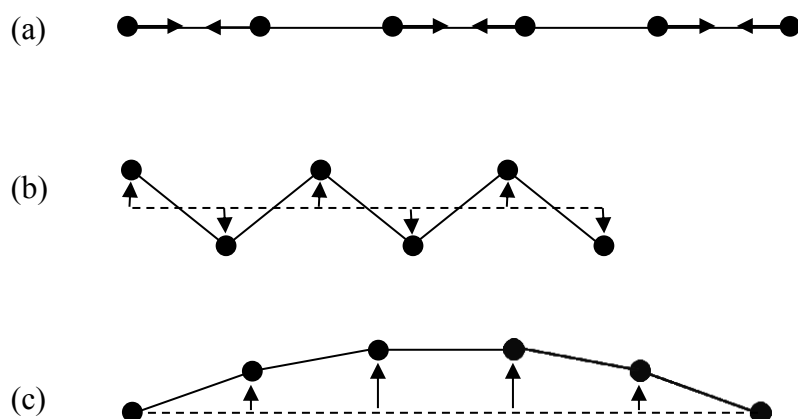


Fig. 2 Schematic illustrations of lattice modes for a chain of atoms. (a) Longitudinal optic (LO) mode leading to PTE through asymmetry of the pairwise bonding potential shown in Fig. 1. (b) High energy transverse optic (TO) mode that greatly shortens the chain giving large NTE as the vibrational amplitude increases with temperature. (c) Low energy transverse acoustic (TA) mode leading to more modest NTE as temperature increases.

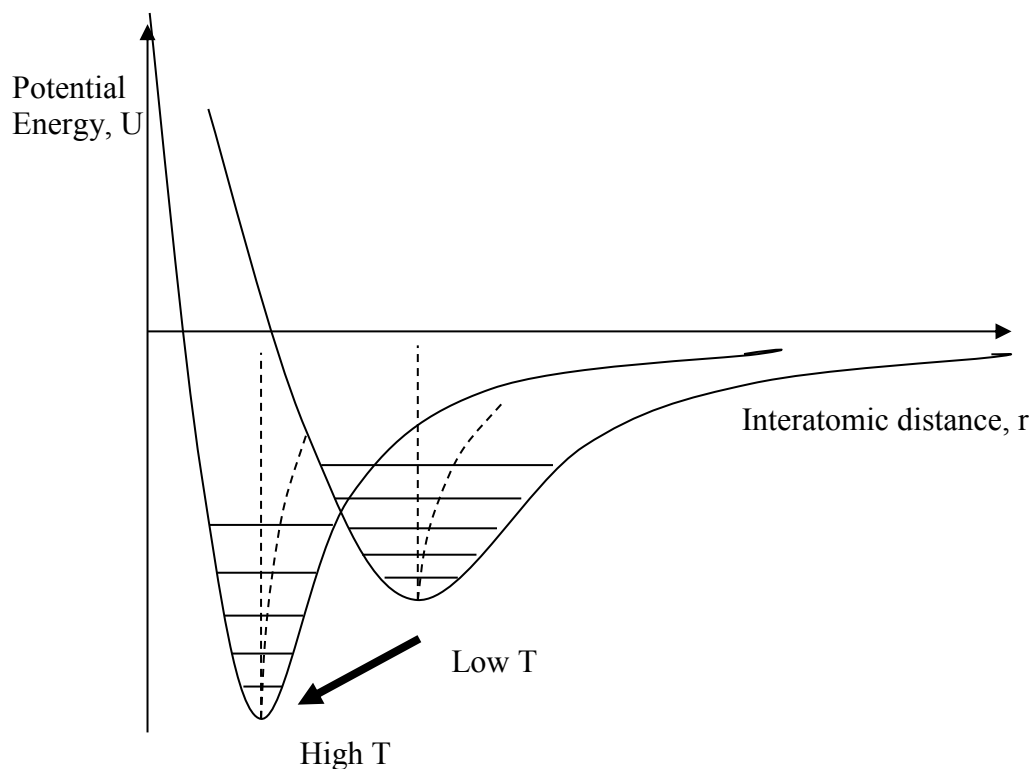


Fig. 3 Illustration of electronic mechanisms for NTE, where the interatomic bonding potential changes with temperature, moving to a more strongly bonding curve with smaller equilibrium distance at higher temperature. This may occur through a relatively sharp first order phase transition between two distinct states, or the potential may gradually evolve with changing temperature.

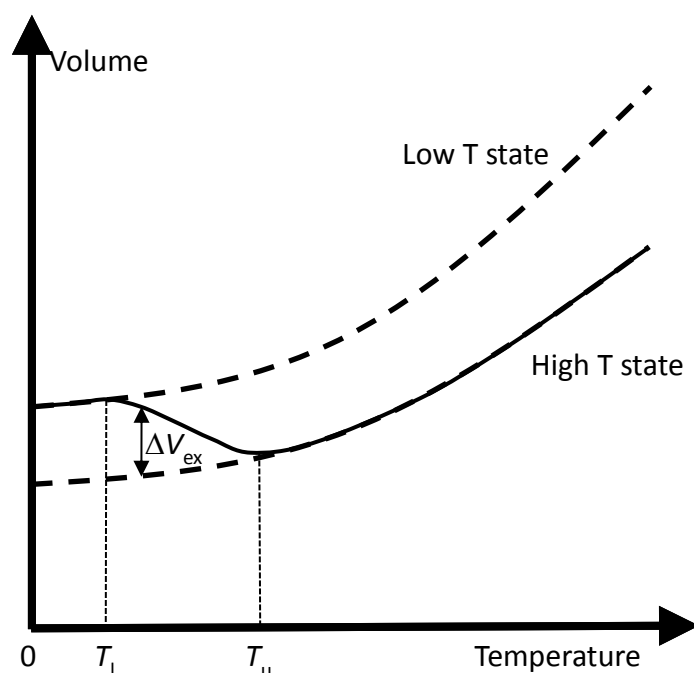


Fig. 4 Schematic changes in lattice volume with temperature for a material displaying electronic NTE. The change from the larger-volume low- T to the smaller-volume high- T states (as shown in Fig. 3) leads to NTE in the crossover region with lower and upper temperatures T_l and T_u . T_u often marks an ordering temperature such as a magnetic or ferroelectric Curie transition. The electronically-induced excess volume ΔV_{ex} relative to the extrapolated volume of the high- T state is shown

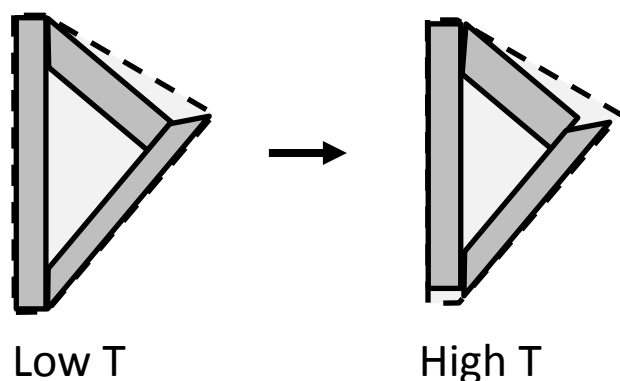


Fig. 5 Illustrative two-dimensional model for the microstructural NTE effect, showing three crystallites enclosing a void. The crystallites shown have contracted by 10% along their long axis and expanded by 10% in the perpendicular direction on changing from low T to high T , so their total area has not changed. However, the enclosing area for the ensemble shown by broken lines undergoes an overall decrease of 8%, illustrating how anisotropic thermal expansion may lead to overall NTE.

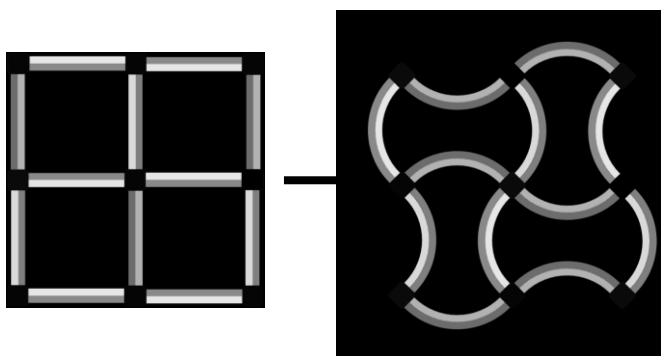
Low T High T

Fig. 6 Illustrative two-dimensional example of an NTE metamaterial consisting of a square lattice of bimaterial strips acting as struts between 4-connected nodes. On heating from the low T to the high T state, the light and dark grey materials respectively expand in length by 6 and 17%, but the separation between nodes decreases by 4% corresponding to an 8% area contraction. Hence the metamaterial consisting of only PTE substances shows bulk NTE.